3D modelling strategy for weather radar data analysis

6 authors, including:

Mingyue Lu
Nanjing University of Information Science & Technology
5 PUBLICATIONS **37** CITATIONS

Min Chen
Key Laboratory of Virtual Geographic Environment, Ministry of Education of PRC
86 PUBLICATIONS **827** CITATIONS

Manzhu Yu
Pennsylvania State University
29 PUBLICATIONS **186** CITATIONS

Yongyao Jiang
George Mason University
21 PUBLICATIONS **138** CITATIONS

Some of the authors of this publication are also working on these related projects:

AIST-MUDROD View project

geospatial cyberinfrastruture View project

3D modelling strategy for weather radar data analysis

Mingyue Lu[1,4] · Min Chen[2,5] · Xinhao Wang[1,4] · Manzhu Yu[3] · Yongyao Jiang[3] · Chaowei Yang[3]

Abstract

Weather radar data, which have obvious spatial characteristics, represent an important and essential data source for weather identification and prediction, and the multi-dimensional visualization and analysis of such data in a three-dimensional (3D) environment are important strategies for meteorological assessments of potentially disastrous weather. The previous studies have generally used regular 3D raster grids as a basic structure to represent radar data and reconstruct convective clouds. However, conducting weather radar data analyses based on regular 3D raster grids is time-consuming and inefficient, because such analyses involve considerable amounts of tedious data interpolation, and they cannot be used to address real-time situ-ations or provide rapid-response solutions. Therefore, a new 3D modelling strategy that can be used to efficiently represent and analyse radar data is proposed in this article. According to the mode by which the radar data are obtained, the proposed 3D modelling strategy organizes the radar data using logical objects entitled radar-point, radar-line, radar-sector, and radar-cluster objects. In these logical objects, the radar point is the basic object that carries the real radar data unit detected from the radar scan, and the radar-line, radar-sector, and radar-cluster objects organize the radar-point collection in different spatial levels that are consistent with the intrinsic spatial structure of the radar scan. Radar points can be regarded as spatial points, and their spatial structure can support logical objects; thus, the radar points can be flexibly connected to construct continuous surface data with quads and volume data with hexahedron cells without additional tedious data interpolation. This model can be used to conduct corresponding operations, such as extracting an isosurface with the marching cube method and a radar profile with a designed sectioning algorithm to represent the outer and inner structure of a convective cloud. Finally, a case study is provided to verify that the proposed 3D modelling strategy has a better performance in radar data analysis and can intuitively and effectively represent the 3D structure of convective clouds.

Keywords Weather radar data · 3D modelling strategy · Convective cloud · Analysis

✉ Min Chen
chenmin0902@163.com

1 Collaborative Innovation Center on Forecast and Evaluation of Meteorological Disasters, Nanjing University of Information Science and Technology, Nanjing 210044, China

2 Key Laboratory of Virtual Geographic Environment, Ministry of Education, Nanjing Normal University, Nanjing 210023, China

3 Geography and GeoInformation Science, George Mason University, Fairfax 22031, USA

4 School of Geography Science, Nanjing University of Information Science and Technology, Nanjing 210044, Jiangsu, China

5 Jiangsu Center for Collaborative Innovation in Geographical Information Resource Development and Application, Nanjing 210023, Jiangsu, China

Introduction

Weather radar data represent an important and essential data source for weather analysis (Fulton et al. 1997; Büyükbas 2005; Geçer 2005; Yu et al. 2006; Wang et al. 2012) and are widely used in meteorological forecasting and weather warnings (Anagnostou et al. 1999; Ciach and Krajewski 1999; Xie et al. 2005; Xu et al. 2010). The traditional methods of performing radar data visualization and analysis are still mostly limited to 2D projected-plane space, which distorts the real status of radar data and cannot effectively represent the real 3D structures of convective clouds (Liu et al. 2017). In fact, radars can detect information throughout the 3D space around itself; therefore, radar data contain 3D characteristics of convective clouds. From this perspective, the 2D-projected mode may neglect considerable valuable information that is hidden in the 3D radar data, thus causing

barriers to data analysis and potential applications. Recently, with the development of geographic information systems (GIS), especially 3D GIS and spatial–temporal GIS (Crum and Alberty 2010; Craglia et al. 2008; Goodchild 2012; Dobesch et al. 2013; Chen et al. 2015; Lü et al. 2018), more research has focused on radar data in 3D space. In addition to radar data 3D visualizations (Ernvik 2002; Oliveira et al. 2014; Guan et al. 2015; Han et al. 2016; Yu et al. 2016), studies have focused on 3D reconstructions of radar data (Zhang et al. 2005; Lu et al. 2013, 2017; Liu et al. 2017). These studies have broadly enhanced the traditional research strategies used for 3D representations of radar data and have helped meteorological specialists to better understand disastrous weather; therefore, their findings can contribute to better decisions. However, most previous research has generally used regular raster grids as the basis to reconstruct convective clouds, although this approach has certain limitations: (1) constructing 3D regular raster grids normally requires a considerable amount of interpolation, which may exhaust computing and memory resources. In actual applications, radar data can cover a circular area with a radius of 460 km and a height of 20 km. If the resolution is 1 km, the 3D grid would contain approximately $920 \times 920 \times 20 = 16,928,000$ cells, and each cell should be filled with a value for subsequent data acquisition and analysis. (2) Because there is a much larger amount of data in the reconstructed 3D raster grids than in the original radar data, the corresponding processes based on the raster grids would involve much more tedious data computations, thus reducing the processing efficiency. Therefore, the traditional studies based on regular raster grids have limitations when applied to addressing real-time situations or generating rapid-response solutions. In this article, the radar volume-scan mode is used to obtain radar data, and a 3D modelling strategy is proposed that uses the radar-point, radar-line, radar-sector, and radar-cluster logical objects instead of regular raster grids. The objective is to provide an effective 3D modelling approach to support the representation and analysis of 3D radar data with high efficiency.

The remainder of this article is structured as follows. The basic idea and the logical radar objects are introduced in "Basic concept and logical radar objects". In "Radar data 3D operation and analysis based on the proposed modelling strategy", the implementation related to the pre-processing and the operation based on the proposed modelling strategy are described, and the advanced analysis is illustrated. Related experiments are described in "Experiment and results", and conclusions and a discussion of directions for further study are presented in "Conclusions and discussion".

Basic concept and logical radar objects

Analysis of a weather radar scan

In applications, weather radar operations are typically performed in volume-scan mode. As indicated in Fig. 1 (Lu et al. 2017), the antenna rotates to generate a full cycle (360°) at one elevation angle. Then, the antenna tilts up a degree and finishes another full cycle (Rinehart 2004; Oliveira et al. 2014). For example, the S-Band Doppler weather radar (Yu et al. 2006) performs 11 sweeps (forming 11 full cycles) in a complete radar volume scan, in which each sweep has approximately 360 rays. In each ray, a number of bins are included within the same gap. The bins here are the basic radar data units. In general, the weather radar can detect three variables: reflectivity, spectral width, and wind radial velocity. In this article, we focus primarily on reflectivity data, which can represent the structure of convective clouds very well. Originally, radar data were spatially recorded in the polar coordinate system, although they can be transferred into a geographic coordinate system based on the position of the radar antenna.

Logical radar objects

As previously mentioned, for the radar volume-scan mode, the spatial position of every bin in the radar data is defined by the elevation and azimuth parameters and the distance to the antenna. Thus, each bin can also be regarded as a specific point attached to a radar value, which is recognized as a radar-point (abbreviated as rPoint in this
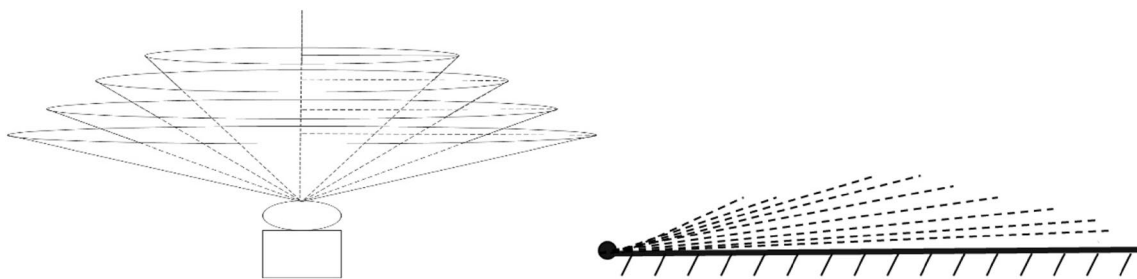

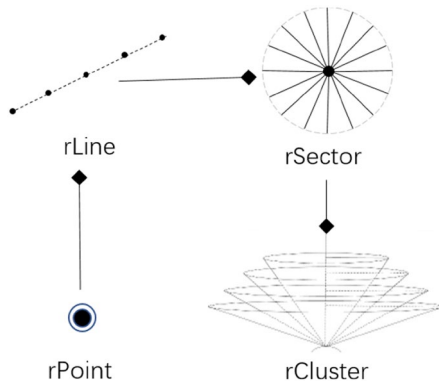**Fig. 1** Volume-scan mode of a weather radar (Lu et al. 2017)

Fig. 2 Logical structure of the 3D modelling strategy

paper). According to the radar volume-scan characteristics, a number of rPoints with the same gap are organized as a radar-line (abbreviated as rLine), and approximately 360 rLines with the same elevation are arranged as a radar sector (abbreviated as rSector). Certain rSectors consist of a radar cluster (abbreviated as rCluster), which is the basic structure of the proposed 3D modelling strategy, in which the rPoint is the basic data unit. This structure is consistent with the intrinsic spatial structure in the radar volume-scan mode. The data objects used in the 3D modelling strategy can be defined separately as follows, and the logical data structure is illustrated as shown in Fig. 2:

$$\text{rPoint} = P(x, y, z, A), \tag{1}$$

where x, y, and z are the coordinates of the rPoint; A is the attributes of the rPoint.

$$\text{rLine} = L(\text{rPoints}, \text{LI}), \tag{2}$$

where rPoints is the rPoints composing the rLine; LI is the attributes of the rLine.

$$\text{rSector} = S(\text{rLines}, \text{SI}), \tag{3}$$

where rLines is the rLines composing the rSector; SI is the attributes of the rSector.

$$\text{rCluster} = C(\text{rSectors}, \text{CI}) \tag{4}$$

where rSectors is the rSectors composing the rCluster; CI is the attributes of the rCluster.

Using the straightforward spatial structure of the logical radar objects, the rPoints, which carry basic radar data units, can be connected to construct other spatial geometry cells, such as line segments, triangles, quads, tetrahedra, and hexahedra. Therefore, based on the real radar data units, tedious 3D raster grids are avoided, and the proposed modelling strategy possesses various potential transformations, such as a surface with quads, thus allowing a volume with hexahedron cells to be represented efficiently and further analyses to be conducted with great flexibility.

Radar data 3D operation and analysis based on the proposed modelling strategy

Radar data pre-processing

In general, in the raw radar data, the number of rLines varies in different rSectors. Thus, different rSectors contain different numbers of rLines. For example, the first rSector may have 366 rLines, and the second rSector may have 368 rLines. Thus, to facilitate subsequent representation and analysis, a pre-process called formalization should be performed to ensure that each rSector contains the same number of rLines with a specified azimuth gap. Naturally, in the process, the key issue is to generate new rLines at certain specified azimuths based on the existing rLines in each rSector through the interpolation method.

As shown in Fig. 3, rLine_1 and rLine_2 are existing rLines beside the target rLine. Because the target rLine is composed of rPoints, the key step is to determine the target rPoints located on the target rLine with their coordinates and attribute values. We suppose that the target rLine has the same number of rPoints and the same distant gaps as rLine1 and rLine2 (actually, if the rLines belong to the same rSector, they have the same number of rPoints). For one target rPoint (P) on the target rLine, the two neighbour rPoints (P_1 and P_2) can be determined on the adjacent existing rLines (rLine1 and rLine2) using their azimuths, which are on two sides of the target rLine. Therefore, the attribute value on the target rPoint (P) can be determined according to the parameters of ΔAz_1 and ΔAz_2, and the values of P_1 and P_2 can be determined according to the following formula:

$$P_{\text{v}} = (P_{\text{v1}} \times \Delta Az_2 + P_{\text{v2}} \times \Delta Az_1)/(\Delta Az_1 + \Delta Az_2),$$

where P_{v} is the value attached to target rPoint P; P_{v1} is the value attached to the existing rPoint P_1; P_{v2} is the value attached to existing rPoint P_2; ΔAz_1 is the angle between the target rLine and the existing rLine_1; ΔAz_2 is the angle between the target rLine and the existing rLine_2.
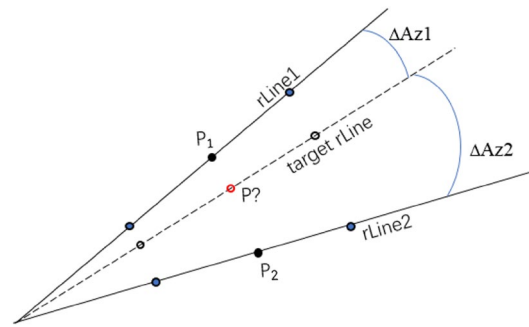

Fig. 3 Schematic diagram of formalization

Similarly, the coordinates of the target rPoint P can also be determined using the following formula:

$$X = (X_1 \times \Delta Az_2 + X_2 \times \Delta Az_1)/(\Delta Az_1 + \Delta Az_2),$$

where X is the coordinates of the target rPoint P; X_1 is the coordinates of the existing rPoint P_1; X_2 is the coordinates of the existing rPoint P_2; ΔAz_1 is the angle between the target rLine and existing rLine$_1$; ΔAz_2 is the angle between the target rLine and existing rLine$_2$.

Thus, all information (coordinates and attributes) regarding target rPoint P can be obtained, and all rPoints on the target rLine can be determined. Therefore, a new rLine with a certain specified azimuth can be generated. In this paper, after formalization, each rSector contains 360 rLines with an azimuth gap of 1°; that is, the azimuth of the first rLine is 0°, the azimuth of the second is 1°, the third is 2°, etc. until the azimuth of the 360th rLine is 359°. Thus, each rLine in the different rSectors can be well matched to a specified azimuth. Therefore, the formalization provides a pathway to subsequent processing.

Volumetric representation of the radar data

Construction of radar volumetric data with hexahedron cells

To construct the radar volumetric data, the volumetric cells that can transfer discrete rPoints to a continuous volume
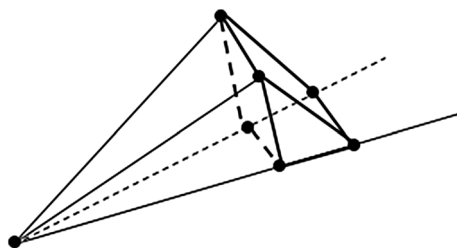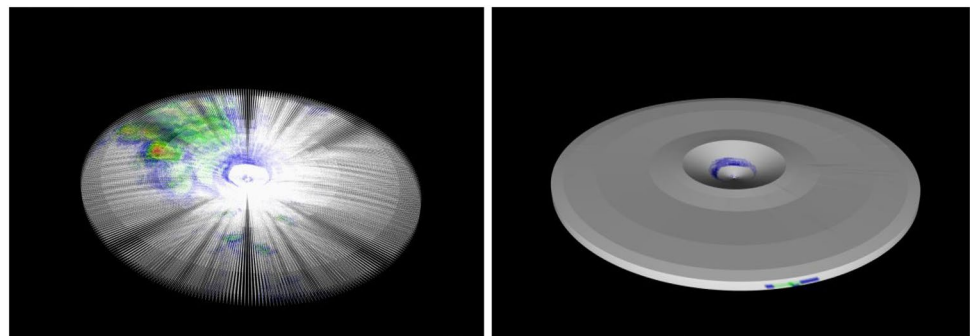

Fig. 4 An alternative strategy for constructing a hexahedron cell using six rPoints

should be constructed first. Therefore, in this paper, the eight adjacent rPoints (four rPoints in the upper rSector and four rPoints in the lower rSector, in which the two rSectors are adjacent) are connected to build a hexahedron, as shown in Fig. 4. In the raw radar data, the numbers of rPoints in each rLine are equal in the same rSector but differ in different rSectors. For example, each rLine may contain 460 rPoints in the first rSector but 370 rPoints in the second rSector. Therefore, in the process of constructing hexahedron cells, two strategies are employed: if the four rPoints in the lower rSector can match the four rPoints in the upper rSector, they can be connected directly, to construct a hexahedron cell; if the number of rPoints in the rLine in the upper rSector is less than those in the lower rSector, then the latter four rPoints in the lower rSector would not correspond to the rPoints in the upper rSector to construct a hexahedron cell. In this situation, an alternative strategy, which is to connect four rPoints in the lower rSector with the last two rPoints in the upper rSector, should be adopted, as shown in Fig. 4. Accordingly, the quadrilateral based on the four rPoints in the upper rSector is degenerated to a line segment, and the hexahedron is degenerated to a triangular prism.

With these strategies, the radar volumetric data based on the hexahedron cells can be constructed successfully, as shown in Fig. 5.

3D isosurface construction

The constructed radar volumetric data are filled with continuous hexahedron cells. Because each hexahedron cell can be regarded as one special cube grid, the entire volume of data arranged with certain regular rules can also be regarded as a special cube grid net. Therefore, the 3D isosurface can be extracted with the marching cubes (MC) algorithm from the constructed radar volumetric data. MC is a representative and widely used method for obtaining isosurfaces in the 3D literature (Rajon and Bolch 2003; Newman et al. 2004; Newman and Yi 2006; Engwer and Nüßing 2017). An isosurface with a certain value can be obtained, as shown in Fig. 6.

Fig. 5 Construction of radar volumetric data based on hexahedron cells

a rPoints in the radar data   **b** Radar volumetric data with hexahedron cells

Fig. 6 3D isosurface extracted from radar hexahedron volumetric data

Fig. 7 Cutting plane defined by a normal vector and a specified point
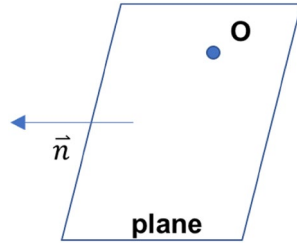
Extracting a profile with an arbitrary cutting plane

Profiles are important for exploring the inner structure of convective clouds. With the proposed modelling strategy, a profile with an arbitrary cutting plane can be extracted directly.

Three steps should be taken to achieve this purpose:

1. Calculate the intersection points between the rLines and the cutting plane;
2. Extract the contour from the intersection points that are scattered on the cutting plane;
3. Fill the contour with different colours according to the values.

We assume that the cutting plane is defined by a normal vector $\vec{n}$ and a specified point (O) on the cutting plane. Then, the cutting plane can be indicated by formula (5) and by Fig. 7:

$$\overrightarrow{PO} \cdot \vec{n} = 0, \tag{5}$$

where P is an arbitrary point on the cutting plane; O is a specified point on the cutting plane; $\overrightarrow{PO}$ is the vector from point P to point O; $\vec{n}$ is the normal vector of the cutting plane.

Thus, this extraction process can be performed based on the following steps.

Step 1: Calculate the intersection points between rLines and the cutting plane.

1. Ensure that an intersection point is placed between an rLine and the cutting plane.

In each rLine, if rPoints occur separately on two sides of the cutting plane, then an intersection would occur between the rLine and the cutting plane. Therefore, we choose the first rPoint as P_1 and the last rPoint as P_2 in an rLine, and if the two rPoints are on the same side of the cutting plane, then an intersection would not occur, although an intersection point would occur with the cutting plane. To identify the relative positions of two rPoints according to the cutting plane, formula (6) is used:

$$(\overrightarrow{OP_1} \cdot \vec{n}) \times (\overrightarrow{OP_2} \cdot \vec{n}) \begin{cases} > 0 \text{ on the same side of the plane} \\ = 0 \text{ at least one point on the plane}, \\ < 0 \text{ on two sides of the plane} \end{cases} \tag{6}$$

where P_1 is the one rPoint on the radar rLine; P_2 is the another rPoint on the radar rLine; $\overrightarrow{OP_1}$ is the vector from O to P_1; $\overrightarrow{OP_2}$ is the vector from O to P_2; $\vec{n}$ is the normal vector of the cutting plane.

2. Determine the two adjacent rPoints on the two sides of the cutting plane in the rLine.

The intersection point must stay between the two rPoints that are adjacent in the radar rLine and occur separately on two sides of the cutting plane. In this paper, the half-interval search method is adopted to find these points. In this method, if P_1 and P_2 exist separately on two sides of the cutting plane, then the rPoint (P) in the middle position of the two rPoints is chosen; if the rPoint P is on the cutting plane, then the rPoint P is the intersection point that we are seeking; and if the rPoint P is on the same side of the cutting plane as P_1, then P_1 is replaced with P; or, P_2 is replaced with P. Then, we continue to identify the relative positions of P_1 and P_2 according to the cutting plane. This process is repeated until P_1 and P_2 are adjacent and on two sides of the cutting plane. The entire process is shown by the flow diagram in Fig. 8.

3. Obtain the actual intersection point with attributes.

After obtaining the two adjacent rPoints (P_1 and P_2), the actual intersection point can be determined with the following method. If either of the two rPoints is only on the plane, then the rPoint on the plane is the intersection point that we are seeking; however, if the interpolation point is P, then its location can be calculated using formula (7):

$$L_1 = \left\| \overrightarrow{OP_1} \cdot \vec{n_0} \right\|$$

$$L_2 = \left\| \overrightarrow{OP_2} \cdot \vec{n_0} \right\|$$

Fig. 8 Flow diagram for the half-interval search method to identify two adjacent rPoints separated on two sides of the cutting plane
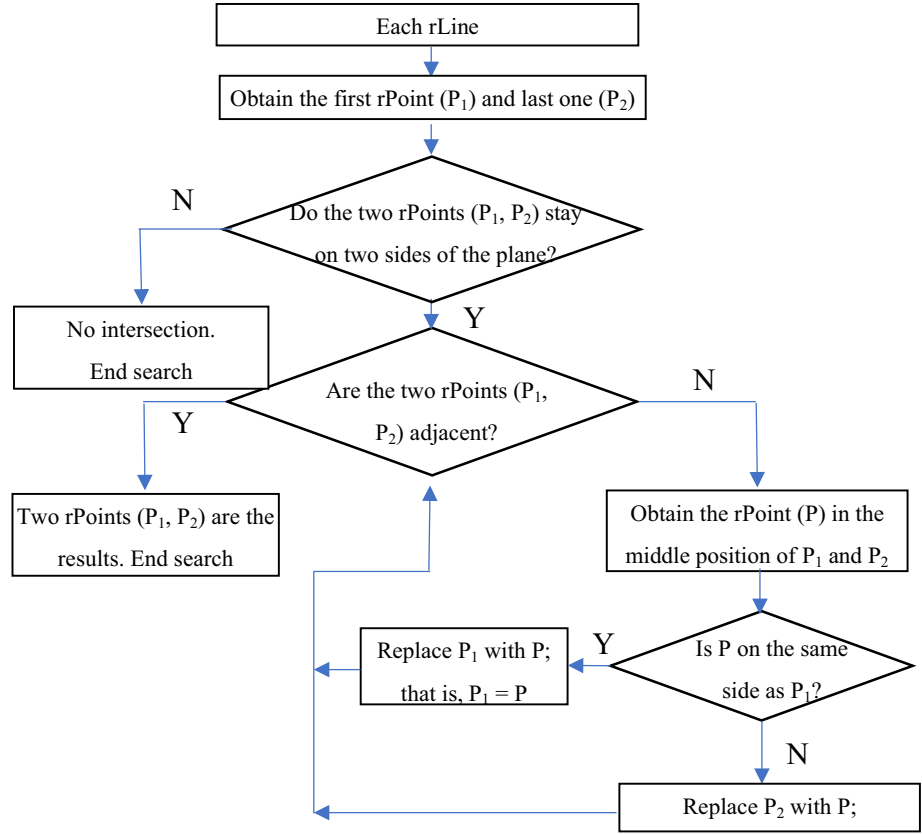
$$P = P_1 + \left(\frac{L_1}{L_1 + L_2}\right) \cdot \overrightarrow{P_1P_2}, \tag{7}$$

where L_1 is the vertical distance from P_1 to the cutting plane; L_2 is the vertical distance from P_2 to the cutting plane; P is the location (coordinates) of the intersection point; $\vec{n}$ is the normal vector of the cutting plane; O is a specified point on the cutting plane; $\overrightarrow{OP_1}$ is the vector from point O to rPoint P_1; $\overrightarrow{OP_2}$ is the vector from point O to rPoint P_2; $\overrightarrow{P_1P_2}$ is the vector from rPoint P_1 to rPoint P_2.

In addition, the attributes (the radar reflectivity value in this paper) of the intersection point can be determined by a linear interpolation between rPoints P_1 and P_2 as indicated by formula (8):
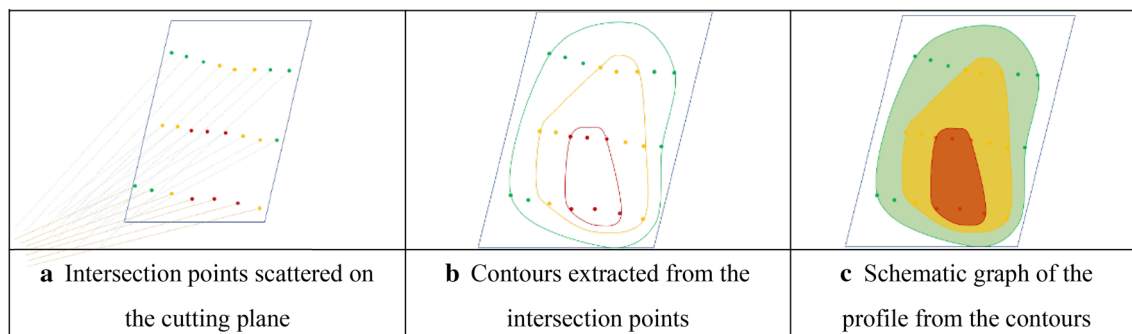
$$Z = \frac{Z_2L_1 + Z_1L_2}{L_1 + L_2}, \tag{8}$$

where Z is the value on the interpolated point; Z_1 is the value on rPoint P_1; Z_2 is the value on rPoint P_2; L_1 is the vertical distance from rPoint P_1 to the cutting plane; L_2 is the vertical distance from rPoint P_2 to the cutting plane.

After performing the above steps, the intersection points with attribute values can be obtained and scattered on the cutting plane. A schematic graph is shown in Fig. 9a.

Step 2: Extract the contours from the intersection points scattered on the cutting plane.

The intersection points containing radar reflectivity information are scattered on the cutting plane. Therefore, a Triangulated Irregular Network (TIN) can be constructed from the points within the cutting plane. Currently, most methods for triangulation are applied in a 2D *XY*-projection scenario, although, in practical applications, the cutting plane may not be the *XY*-projection plane; therefore, a transformation must be performed before the traditional methods can be used in a 3D scenario. In this paper, we check the normal vector of the cutting plane. If the *X*-axis in the coordinate system is more parallel with the normal vector than the *Y*- and *Z*-axes, all points should exchange their *X* coordinate value with their *Z*-coordinate value, whereas if the *Y*-axis in the coordinate system is more parallel with the normal vector than the *X*- and *Z*-axes, then all points should exchange their *Y* coordinate value with their *Z*-coordinate value; otherwise, no exchange is needed. Subsequently, we can triangulate the points using a regular triangulation method involving *X*- and *Y*-coordinates but not the *Z*-coordinate value. Finally, after finishing the triangulation process, all points' coordinates in the TIN data should be exchanged back to their original state (that is, if the points were exchanged from the *X* value to the *Z* value, then they should be exchanged back). Thus,

| **a** Intersection points scattered on the cutting plane | **b** Contours extracted from the intersection points | **c** Schematic graph of the profile from the contours |

Fig. 9 Schematic graph for the construction of a profile based on the 3D modelling strategy

the TIN data are successfully constructed. With the support of TIN data, the contours of a series of values can be extracted via the same strategy. A schematic graph is shown in Fig. 9b.

Step 3: Fill the contours and achieve the profile.

All extracted contours are closed polylines, which should be transformed into polygons and filled with a series of colours within the cutting plane to indicate different radar reflectivity values. During this procedure, the topological relationship should be checked; that is, the relationship among the contour polylines should be clarified. According to the characteristics of the contour, if one point of a contour polyline (CP_1) is contained in another contour polyline (CP_2), then the entire CP_1 must be contained in CP_2. Considering this characteristic, the issue is simplified to a problem of whether a closed polyline contains a point. This issue is common in 2D fields. In this paper, all the contours remain in 3D space, although they are still in the same spatial plane. Therefore, certain modifications are adopted in this paper to solve this problem according to the following steps:

1. Choose a point P_1 in CP_1 and a point P_2 in CP_2.
2. Construct a vector ($\vec{v}$) from P_1 to P_2, and the vector rLine equation can be defined as follows:

$$R = P_1 + \vec{v}t \quad (t \geqslant 0),$$

where R is an arbitrary point on the rLine; P_1 is the point on CP_1; $\vec{v}$ is a vector from P_1 to P_2; t is a parameter in the equation; here, $t \geq 0$.

3. Determine the intersection count between the vector rLine and contour polyline CP_2 via the above equation. The following judgement is similar to the regular method for 2D fields. If the count is odd, then the point is contained in CP_2; otherwise, the point is not contained.

After the topological relationship is confirmed through these steps, the contour polygons can be obtained, and the profile is achieved, as shown in Fig. 9c.

Experiment and results

An experiment was performed to verify the applicability and efficiency of the proposed 3D modelling strategy for radar data representation and analysis. In this experiment, a Virtual Weather Earth System (VWES) was built based on the browser/server (B/S) architecture to represent and analyse meteorological data in a virtual 3D geo-environment. On the server side, the radar data modelling approach and the algorithms were implemented using the Java computer language and deployed as service interfaces. On the browser side, a webpage-based 3D earth system was developed using the JavaScript computer language for operations and interactions by the user. When the user submits requests to the radar product, the service interfaces start the corresponding algorithm to address the specified radar data and transfer the resulting data to the browser for display.

In this experiment, raw radar data of a convective cloud that occurred in Jiangsu Province, China, were adopted for testing. First, the radar-point data were requested from the browser; then, on the server side, the specified raw radar data were parsed from a radar binary file, and the rPoints containing radar reflectivity information were extracted, pre-processed, and then organized with the rLine, rSector, and rCluster structure. Thus, all the radar-point data were transferred to the browser and displayed, as shown in Fig. 10a (different colours represent different radar reflectivity values). Second, to show the 3D structure of the observed convective cloud, a 3D isosurface with a reflectivity value of 50 DBZ was requested. Then, on the server side, based on the well-structured rPoints, a hexahedron grid network was constructed using the approach proposed in this paper, and

| **(a)** rPoints extracted from the raw data file. | **a** 3D isosurface | **b** vertical profile |
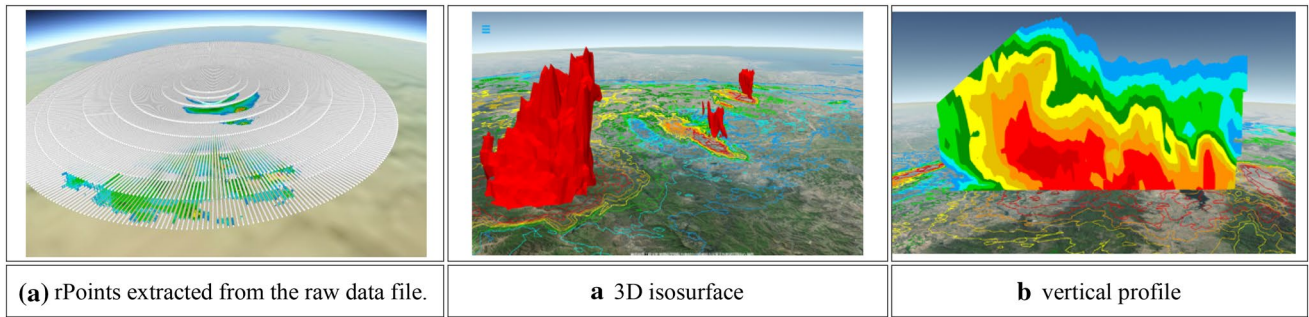
Fig. 10 3D structure of the observed convective cloud represented by the proposed modelling strategy

| **a** the isosurface from the traditional method | **b** profile from the traditional method |
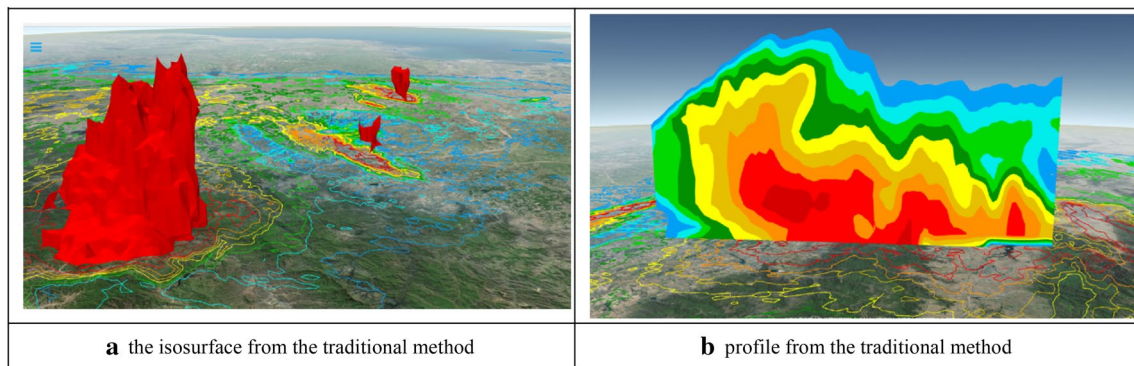
Fig. 11 3D structure of the observed convective cloud represented using the traditional methods

the 3D isosurface was extracted from the network. Thus, the 3D structure was well represented, as shown in Fig. 10b [to obtain a better effect, the contours of the radar composite reflectivity (CR) were also requested and displayed together with the 3D isosurface]. Third, a vertical profile was requested on the browser side to show the inner structure of the observed convective cloud. Thus, the corresponding service of a profile algorithm was started on the server side, the profile was constructed based on the algorithm mentioned above, and the data were transferred to the browser and displayed together with the radar CR contour data, as shown in Fig. 10c.

In the experiment, rapid responses are provided for all the requests, and the user operations are smooth.

Due to the intrinsic object structure of the proposed modelling strategy, algorithms based on the strategy involve less cells than traditional methods do; therefore, fewer computing tasks are involved in the proposed methodology, which makes the rapid response possible in practical operations. In the traditional method, all data are interpolated onto regular grids with a typical resolution of 1 km; thus, more interpolation operations and grid cells are involved in the computing tasks. For comparison, the operations based on the traditional methods are also conducted in this paper, and the resulting data of the

Table 1 Comparison of the time required for the traditional and proposed approaches

Algorithm	Sample size	Average time required for the traditional method (s)	Average time required for the proposed method (s)
Isosurface	10	11.2503	2.1088
Profile	10	4.805	1.280

3D isosurface and profile are displayed in Fig. 11. The products of the proposed and traditional methods are very close; some small differences are acceptable in the field of meteorology. This finding can also verify the validity of the proposed methodology from another aspect. Meanwhile, the operation times of the proposed and traditional methods are listed in Table 1. To obtain the 3D isosurface, the method based on the proposed modelling strategy requires 2.1088 s (average of ten instances), while that based on the traditional method requires 11.2503 s (average of ten instances); to obtain the profile, the required time is 1280 ms (average of ten instances) for the proposed method compared with 4805 ms (average of ten instances) for the traditional method. Table 1 indicates

that the proposed methodology has higher efficiency than the traditional methodology.

Conclusions and discussion

In this paper, a new 3D modelling strategy is proposed to represent and analyse weather radar data based on logical objects, including the rPoint, rLine, rSector, and rCluster. The algorithms of 3D isosurface construction and profile extraction based on the modelling strategy are also described in this paper. Taking advantage of the logical objects structure being consistent with the intrinsic structure of the radar volume-scan mode, 3D algorithms based on the modelling strategy can achieve much higher operating efficiency without a loss in accuracy, because no extra interpolation is required, which differs from the traditional methods. A case study verifies the applicability and effectiveness of the proposed 3D modelling strategy for weather radar data representation and analysis. Comparisons with the traditional methods are also provided in this paper to indicate the efficiency and the potential of the proposed methodology for addressing real-time situations and rapid-response solutions.

With the development of GIS, especially 3D GIS, additional methods and algorithms can be provided to address meteorological data more efficiently based on GIS and to further change the traditional perspective found in the meteorological literature. In the proposed modelling strategy, the rPoint is the basic radar data unit, and an rPoint can be regarded as a special point with an attribute value. Therefore, the strategy inherits the point's advantages and possesses the considerable flexibility of representing various objects in the real world via transformation to other geometric cells (such as lines, triangles, quads, and hexahedra). Moreover, an rPoint can also be linked with a timestamp to record various statuses at different times. In fact, radar data contain obvious spatiotemporal characteristics, and in the raw radar data, each rLine has a timestamp that indicates when it occurred. Therefore, the 3D modelling strategy proposed in this paper has considerable potential to represent spatiotemporal weather processes in the meteorological literature. Thus, the 3D modelling strategy with a temporal stamp (i.e., the spatiotemporal modelling strategy) that includes efficient and effective presentation and analysis methods will be used as a next step for further research to represent and analyse dynamic radar data and disastrous weather processes.

References

Anagnostou EN, Krajewski WF, Smith J (1999) Un-certainty quantification of mean-areal radar-rainfall estimates. J Atmos Ocean Technol 16(2):206–215

Büyükbas E (2005) Training course on weather radar systems. Module A: introduction to radar. WMO, Balıkesir

Chen M, Lin H, Kolditz O, Chen C (2015) Developing dynamic virtual geographic environments (VGEs) for geographic research. Environ Earth Sci 74(10):6975–6980

Ciach GJ, Krajewski WF (1999) Radar-rain gauge comparisons under observational uncertainties. J Appl Meteorol 38(38):1519–1525

Craglia M, Goodchild MF, Annoni A, Camara G, Gould M, Kuhn W, Mark D, Masser I et al (2008) Next-generation digital earth—a position paper from the vespucci initiative for the advancement of geographic information science. Int J Spat Data Infrastruct Res 3:146–167

Crum TD, Alberty RL (2010) The WSR-88D and the WSR-88D operational support facility. Bull Am Meteorol Soc 74(9):1669–1687

Dobesch H, Dumolard P, Dyras I (2013) Spatial interpolation for climate data-the use of GIS in climatology and meteorology. ISTE Ltd, London

Engwer C, Nüßing A (2017) Geometric reconstruction of implicitly defined surfaces and domains with topological guarantees. ACM Trans Math Softw. https://doi.org/10.1145/3104989

Ernvik A (2002) 3D visualization of weather radar data. Master's thesis, Linköping University

Fulton RA, Breidenbach JP, Seo DJ, Miller DA, O'Bannon T (1997) The WSR-88D rainfall algorithm. Weather Forecast 13(2):377–395

Geçer C (2005) Training course on weather radar systems. Module D: radar products and operational applications. WMO, Balıkesir

Goodchild MF (2012) The future of digital earth. Ann GIS 18(2):93–98

Guan L, Wei M, Wei K, Wang J (2015) 3D visualization of doppler radar data based on MATLAB platform. J Henan Norm Univ 43:43–48

Han Y, Liu X, Lu X, Li H (2016) The 3D modeling and radar simulation of low-altitude wind shear via computational fluid dynamics method. In: 2016 Integrated Communications Navigation and Surveillance (ICNS), April. https://ieeexplore.ieee.org/stamp/stamp.jsp?tp=&arnumber=7486349. Accessed 10 Dec 2018

Liu ZN, Shi ZZ, Jiang MR, Zhang J, Chen LQ, Zhang T, Liu GQ (2017) Using MC algorithm to implement 3D Image reconstruction for Yunnan weather radar data. J Comput Commun 5(5):50–61

Lu ZY, Jin X, Han CY (2013) 3D reconstruction of strong convective cell based on doppler radar base data. In: International conference on machine learning and cybernetics IEEE, vol 2, Tianjin, China, pp 845–849

Lu MY, Chen M, Wang X, Min JZ, Liu AL (2017) A spatial lattice model applied for meteorological visualization and analysis. ISPRS Int J GeoInf 6(3):77–90

Lü GN, Chen M, Yuan LW, Zhou LC, Wen YN, Wu MG, Hu B, Yu ZY et al (2018) Geographic scenario: a possible foundation for further development of virtual geographic environments. Int J Digit Earth 11(4):356–368

Newman TS, Yi H (2006) A survey of the marching cubes algorithm. Comput Graph 30(5):854–879

Newman TS, Byrd JB, Emani P, Narayanan A, Dastmalchi A (2004) High performance SIMD marching cubes isosurface extraction on commodity computers. Comput Graph 28(2):213–233

Oliveira Jr, Abimael A, Sérgio S, Fábio S (2014) 3D visualization tool for meteorological radar data using WebGL. In: 10th world congress on computational mechanics, May, vol 1, no 1. http://www.proceedings.blucher.com.br/evento/10wccm. Accessed 10 Dec 2018

Rajon DA, Bolch WE (2003) Marching cube algorithm: review and trilinear interpolation adaptation for image-based dosimetric models. Comput Med Imaging Graph 27(5):411–435

Rinehart R (2004) Radar for meteorologists. Rinehart Publications, New York

Wang P, Xu KJ, Zhang Y, Jia HZ (2012) Doppler weather radar clutter suppression based on texture feature. In: Proceedings of the 2012 international conference on machine learning and cybernetics, Xian, 15–17 July 2012, pp 1339–1344

Xie HJ, Zhou XB, Vivoni ER, Hendrickx JMH, Small EE (2005) GIS-based NEXRAD Stage III precipitation database: automated approaches for data processing and visualization. Comput Geosci 31(1):65–76

Xu WX, Li GD, Liao FJ (2010) Forecast hail by analysis radar image. In: Proceedings of the ninth international conference on machine learning and cybernetics, Qingdao, 11–14 July 2010, pp 730–734

Yu YJ, Li Y (2016) Method for detecting and simulating 3D turbulence field of airborne weather radar. Syst Eng Electron 38:293–297

Yu XD, Yao XP, Xiong YN (2006) Doppler weather radar principles and business applications. Meteorological Press, Beijing

Zhang J, Howard K, Gourley JJ (2005) Constructing three-dimensional multiple-radar reflectivity mosaics: examples of convective storms and stratiform rain echoes. J Atmos Ocean Technol 22(1):30–42